Superlattices and Microstructures 146 (2020) 106658

Contents lists available at ScienceDirect

Superlattices and Microstructures

journal homepage: www.elsevier.com/locate/superlattices

Investigation of electrical parameters of Au/P3HT:PCBM/n-6H–SiC/Ag Schottky barrier diode with different current conduction models

Hayati Altan [a], Metin Özer [a,*], Hüseyin Ezgin [b]

[a] Department of Physics, Gazi University, Ankara 06500, Turkey
[b] Department of Advanced Technologies, Gazi University, Ankara 06500, Turkey

ARTICLE INFO

Keywords:
Schottky barrier diode
n-6H–SiC
P3HT:PCBM
Gaussian distribution
Effective Richardson constant
Inhomogeneous barrier height

ABSTRACT

We have researched the electrical characteristics of Au/P3HT:PCBM/n-6H–SiC/Ag Schottky barrier diode (SBD) fabricated with a polymer interface layer between 300 and 375 K temperatures. The experimentally obtained parameters from current-voltage (I–V) measurements are calculated with four different current conduction models. It is observed that parameters calculated from research findings related to different methods are compatible with each other. The barrier inhomogeneity of the metal-polymer-semiconductor (MPS) interface layer is explained by Gaussian distribution (GD). Furthermore, the mean barrier height ($\overline{\Phi}_{bo}$) and the modified effective Richardson constant (A**) are found by drawing Richardson curves of the sample. Finally, the electrical properties of Au/P3HT:PCBM/n-6H–SiC/Ag SBD have been determined to affect the interface materials and the interface state density (N_{ss}) as well as the current conduction models.

1. Introduction

A conventional Schottky barrier diode (SBD) is formed by semiconductor sandwiched between two metals in metal-semiconductor (MS) contact [1]. MS structures provide the basis for semiconductor-based circuit elements and a better understanding of electronic devices in the semiconductor and optoelectronic applications. The formation of an MS potential barrier, the factors affecting this barrier, current conduction mechanisms and their relations with temperature have not been fully illuminated yet [2]. The features of SBDs undergo change depending on metal's work function, type and doping concentration of semiconductor, the bandgap of intrinsic semiconductor [3].

Metal-silicon carbide (M-SiC) contacts are one of the most interesting subjects in potential barrier formation with appropriate interface conditions [4]. M-SiC structures are of great importance due to the physical and electrical properties of contacts [5]. Thanks to these features, M-SiC structures are very suitable for high power and frequency, low and high temperature applications. M-SiC contacts with potential barrier provide several advantages in many applications that cannot be achieved with silicone. Using M-SiC in power electronics could provide lighter, smaller and electrically more efficient systems than conventional M-Si based electronic systems [6]. M-SiC is used significantly in the construction of devices in solar cells, transistors, sensors, defense and space technologies [7–9]. It is also used in laser diodes, light emitting diodes (LED) and as a photodetector in the optoelectronics industry [10–13].

The formation of Schottky contacts has been investigated by many research groups using various metals on n-6H–SiC. Moreover,

* Corresponding author.
E-mail addresses: hayatialtansene@gmail.com (H. Altan), metinoz@gazi.edu.tr (M. Özer), huseyin.ezgin@gazi.edu.tr (H. Ezgin).

https://doi.org/10.1016/j.spmi.2020.106658
Received 9 April 2020; Received in revised form 15 July 2020; Accepted 21 July 2020
Available online 29 July 2020
0749-6036/© 2020 Elsevier Ltd. All rights reserved.

some researchers have conducted in detail studies on the temperature-related electrical parameters of metal/6H–SiC semiconductor SBDs. In these studies, they have reported the temperature dependence of electrical properties calculated using the I–V analysis of metal/n-6H–SiC Schottky barrier diodes. Benemara et al. sought for the temperature-dependent interface state characterization of Ni/6H–SiC SBD at 77–450 K temperature range [6]. Asubay et al. probed the electrical properties of Mo/n-6H–SiC Schottky barrier diode produced by a DC sputtering method at room temperature. They have reported that the inconsistency in barrier heights are ascribed to potential fluctuations in the metal/semiconductor interface [14]. Ejderha et al. studied the electrical properties of Ni/n-6H–SiC Schottky barrier diodes at 40–400 K temperature range [15]. They have explained that the current flows through the lower barrier heights as the temperature decreases because of the inhomogeneous barrier. They have reported the analysis of characteristics of $I(V_G)$ as a function of temperature for this diode. Boussouar et al. researched the electrical features for Mo/4H–SiC Schottky diodes at 303–498 K temperature range [16]. They have reported that the presence of inhomogeneities for the electrical features of Schottky contacts in forward and reverse bias. Güzel et al. made a survey of the existence of inhomogeneous barrier height and the electrical characteristics of Au/6H–SiC MS Schottky diodes at 80–400 K temperature range [17]. They have reported that the inhomogeneity of the barrier height had different standard deviation values at different temperatures.

Metal-polymer-semiconductor (MPS) structures in Schottky diodes are obtained by using polymer materials as the interface layer. MPS structures come to the forefront when compared to other SBD construction types due to their advantages in industrial applications [18]. Using P3HT:PCBM blend as polymeric interface layer in MPS structures can significantly enhance the electrical properties of Schottky barrier diodes. The blend of poly (3-hexylthiophene) (P3HT) and [6,6]-phenyl C61 butyric acid methyl ester (PCBM) offers unique application possibilities in the industry, especially in the field of organic photovoltaics [19,20]. P3HT, a conductive polymer, acts as an electron donor and PCBM, the derivative of fullerene, acts as an electron acceptor [21]. P3HT:PCBM is superior to other organic compounds due to its properties such as light mass, a flexible substrate, low processing cost, and wide usage area [22].

Previous studies have been conducted on the electrical properties of Au/P3HT:PCBM/n-Si SBDs at room temperature. Özmen investigated the electrical parameters of Au/P3HT:PCBM/n-Si structures with different PCBM concentrations at room temperature [23]. PCBM concentrations in P3HT:PCBM blends have been shown to affect the electrical properties of the Schottky barrier diode. In this study have reported that the decrease in the interface state density due to the increase in PCBM concentration can be attributed to higher mobility of charge carriers and to lower barrier heights in the metal/polymer interface. Özmen et al. studied the electrical and the interfacial features of Au/P3HT:PCBM/n-Si SBDs at room temperature [24]. They have reported that P3HT:PCBM polymer interface affected the electrical properties of this diode such as series resistance and interface state density.

As far as we can see from the literature, no study has been found to investigate I–V characteristics of SBDs above room temperature using P3HT:PCBM polymer as the interface layer of M-SiC for the fabricated sample.

In this work, the barrier height inhomogeneity of Au/P3HT:PCBM/n-6H–SiC/Ag structure have researched at 300–375 K temperature range in steps of 15 K. Fundamental electrical parameters such as ideality factor (n), barrier height (Φ_{b0}), series resistance (R_s), interface state density (N_{ss}) and modified effective Richardson constant (A**) determined from I–V plot have calculated by different current conduction models.

2. Experimental

To produce the Schottky barrier diode, the n-6H–SiC semiconductor wafer with 1-inch radius (0001) orientation, 2.6×10^{17} cm^{-3} donor concentration and 280 μm thickness supplied from Cree Inc. as a substrate material was used. To remove organic and other heavy metal contaminations that may occur on the surfaces of this substrate and to eliminate the roughness on the surface, semiconductor material was chemically cleaned in different stages in the ultrasonic bath. It was washed in trichlor ethylene (C_2HCl_3), acetone (C_3H_6O) and methanol (CH_3OH) respectively for 5 min in an ultrasonic vibration bath. After each washing, plentifully immersed in deionized (DI) water and rinsed with shaking. Later, it was held for 10 s in the semiconductor sample $HF + H_2O$ (1:10) solution to annihilate the natural oxide layer on the surface. Chemically cleaned semiconductor material was dried with nitrogen gas

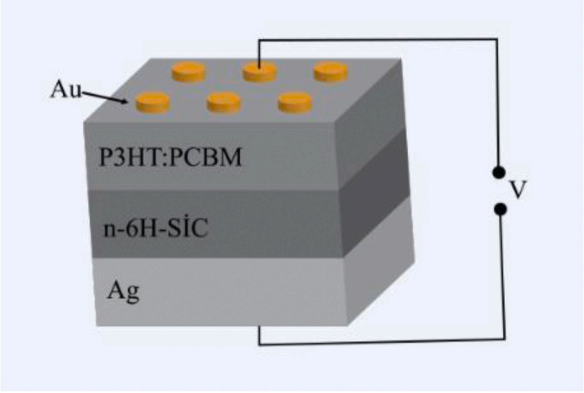

Fig. 1. The cross-sectional view of fabricated Au/P3HT:PCBM/n-6H–SiC/Ag structure.

(99.99%). To form an ohmic contact, the back surface of semiconductor was placed on the mask, the inside of which is empty. When the vacuum reached 6×10^{-6} mbar, chemically cleaned silver (Ag) metal particles with a purity of 99.995% were evaporated by passing current over one of the filaments. The back surface of the semiconductor was coated with a 200 nm thick Ag film using a thickness monitor. After this process, it was kept at 450 °C for 5 min under the same atmosphere and pressure. In this way, Ag film was deposited on the semiconductor. The four-point method was used to determine whether the contact formed is ohmic. On the other hand, P3HT and PCBM with a rate of 25 mg/1 mL were prepared separately by dissolving in chlorobenzene. Each solution was blended with a magnetic stirrer for 2 h and a homogeneous structure was obtained. After liquids were blended with vibration in the ultrasonic bath for 30 min, 150 μL P3HT + 150 μL PCBM (1:1) solution was prepared. The prepared polymer solution was dropped on the n-6H–SiC substrate and put in the spin coating system. The sample was rotated at 750 revolutions per minute (rpm). Here, rpm determines the polymer thickness. The polymer-coated surface of the sample was kept down and 1.5 mm diameter holes were placed on the stainless steel mask with holes drilled. Chemically cleaned pure Au (99.95%) metal piece placed on the filament was evaporated in a vacuum of approximately 10^{-6} mbar and polymer surface of the sample was coated 200 nm thick gold in the form of small circles (1.5 mm in diameter). I–V properties of the sample at 300–375 K temperature range with steps of 15 K were measured using Keithley 2400 Sourcemeter. As a result of measurements, the sample indicated the best diode characteristic of current-voltage values between –3 V and +3 V voltages and current-voltage calculations were taken within these ranges. The cross-sectional view of fabricated Au/P3HT:PCBM/n-6H–SiC/Ag metal-polymer-semiconductor (MPS) SBD structure is shown in Fig. 1.

3. Results and discussion

The representation of the experimental semi-logarithmic forward bias I–V characteristics of Au/P3HT:PCBM/n-6H–SiC/Ag structure at 300–375 K temperature range is represented in Fig. 2. In the case of forward bias, the relationship of current with series resistance in SBD is described by the theory of thermionic emission (TE) as following [25],

$$I = I_0\left[exp\left(\frac{q(V - IR_s)}{nkT}\right) - 1\right], \tag{1}$$

in which electronic charge is q, the ideality factor is n, Boltzmann constant is k, the value of temperature in the term of Kelvin is T, saturation current is I_0 and this parameter is

$$I_0 = AA^*T^2\, exp\left(\frac{-q\Phi_b}{kT}\right), \tag{2}$$

in which the barrier height is Φ_b, the contact area is A, Richardson constant is A*. The theoretically calculated A* value for 6H–SiC is 146 $Acm^{-2}K^{-2}$ [26]. If I_0 in Eq. (2) is put into Eq. (1), the barrier height in Eq. (3) is expressed by

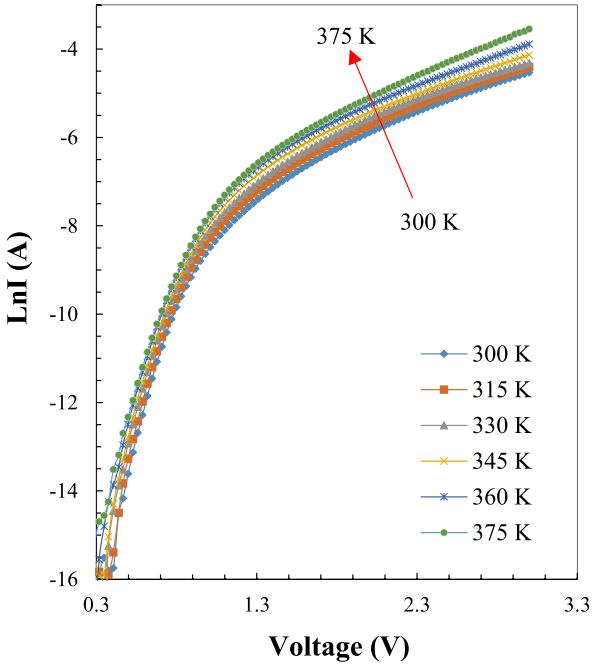

Fig. 2. The semi-log forward bias I–V characteristics of Au/P3HT:PCBM/n-6H–SiC/Ag MPS SBD at different temperatures.

$$\Phi_b = \frac{kT}{q}\, ln\left(\frac{AA^{*}T^{2}}{I_0}\right), \tag{3}$$

The ideality factor is gained from the slope of LnI versus voltage plot. Using Eq. (1), the value of n can be obtained as

$$n = \frac{q}{kT}\left(\frac{d(V - IR_s)}{d(LnI)}\right), \tag{4}$$

The values of n and Φ_b between 300 and 375 K temperatures calculated using Eq. (3) and Eq. (4) are exhibited in Table 1. The ideality factor at 300 K and 375 K temperatures are found as 3.93 and 3.50, respectively. Also, the values of Φ_b calculated at the same temperatures are found as 0.77 eV and 0.94 eV, respectively.

It is seen in Fig. 3 that the values of n decrease and the values of Φ_b increase as the temperature increases. There is an inverse relation between n and Φ_b values. Since current conduction in metal-semiconductor interface depends on temperature, the current at room temperature occurs in regions with lower barrier heights. As the temperature increases, the number of electrons that can exceed barrier height increases. Therefore, barrier height decreases while ideality factor increases [27,28]. The reason for this situation at lower temperatures of measured temperature range is that charge distribution in the interface region is irregular and barrier height of interface consists of different barrier heights [16,29]. According to Fig. 2, as linearity is seen in forward bias region at lower voltages and deviation from linearity is observed at higher voltages. A major cause of this deviation is the series resistance (R_s) [30,31].

R_s is an important parameter for the electrical properties of Schottky diodes. Current conduction mechanism becomes directly related to R_s. The series resistance is acquired from a nonlinear region of I–V plot using a method developed by Cheung and Cheung and is described by following equations [32],

$$\frac{dV}{d(lnI)} = \frac{nkT}{q} + IR_s, \tag{5}$$

$$H(I) = IR_s + n\Phi_{b0}. \tag{6}$$

The experimentally derived dV/dlnI and H(I) versus current (I) plots are given in Fig. 4. These plots are expected to give a linear straight line. According to data derived from Eq. (5), the slope of the plot in Fig. 4(a) gives R_s while the intersection of this plot on y-axis gives n. The series resistance at 300 K and 375 K are found as 492.06 Ω and 210.33 Ω, respectively. The ideality factories at the same temperatures found as 4.75 and 3.43, respectively. According to the data derived from Eq. (6), the slope of the plot in Fig. 4(b) gives the series resistance while the intersection of this plot on the y-axis gives barrier height. The series resistance at 300 K and 375 K are found as 203.74 Ω and 97.27 Ω, respectively. The barrier height at the same temperatures is found as 0.75 eV and 0.94 eV, respectively.

Norde method is another proposed method for finding the series resistance [30]. Difficulties in defining minimum points are disadvantage of this method. Norde function is known as F(V) and is defined by

$$F(V) = \frac{V}{\gamma} - \frac{kT}{q} ln\left(\frac{I(V)}{AA^{*}T^{2}}\right), \tag{7}$$

in which γ is a dimensionless and arbitrary integer value larger than the ideality factor. Norde function versus voltage plot obtained from Eq. (7) is presented in Fig. 5. Additionally, the barrier height in Norde method is determined by Eq. (8),

$$\Phi_b = F_{min} + \frac{V_{min}}{\gamma} - \frac{kT}{q}, \tag{8}$$

in which the minimum F value corresponds to a minimum voltage (V_{min}). The value of series resistance defined by Norde method can be found as

$$R_s = \frac{kT(\gamma - n)}{qI_{min}}, \tag{9}$$

where the minimum current (I_{min}) corresponds to a minimum voltage (V_{min}). The values of R_s calculated from Eq. (9) at 300 K and 375 K are found as 393.87 Ω and 174.89 Ω, respectively. In this study, R_s values calculated using the Cheung-Cheung and Norde methods show good compatibility with each other. In both methods, a decrease in series resistance with increasing temperature for Au/P3HT:

Table 1
The characteristic derived parameters from I–V measurements for Au/P3HT:PCBM/n-6H–SiC/Ag MPS SBD at 300–375 K temperature range.

T (K)	Φ_{b0} (eV)	n (I–V)	n dV/dln(I)–I	R(Ω) dV/dln(I)	R(Ω) H(I)–I	R(Ω) F(V)–V	I_0 (A)
300	0.77	3.93	4.75	492.06	203.74	393.87	2.06E-8
315	0.80	3.83	4.38	403.82	178.70	311.73	2.93E-8
330	0.84	3.64	4.32	324.00	137.30	264.01	3.48E-8
345	0.87	3.62	4.03	266.57	127.69	228.17	5.36E-8
360	0.90	3.55	3.57	242.26	119.23	219.50	7.40E-8
375	0.94	3.50	3.43	210.33	97.27	174.89	9.49E-8

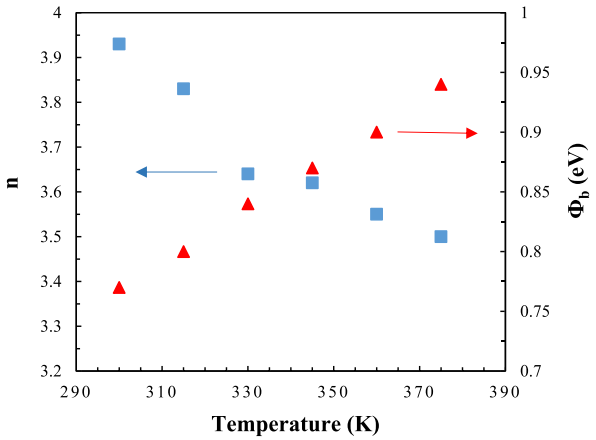

Fig. 3. The variation of n and Φ_b with temperature for Au/P3HT:PCBM/n-6H–SiC/Ag MPS SBD.

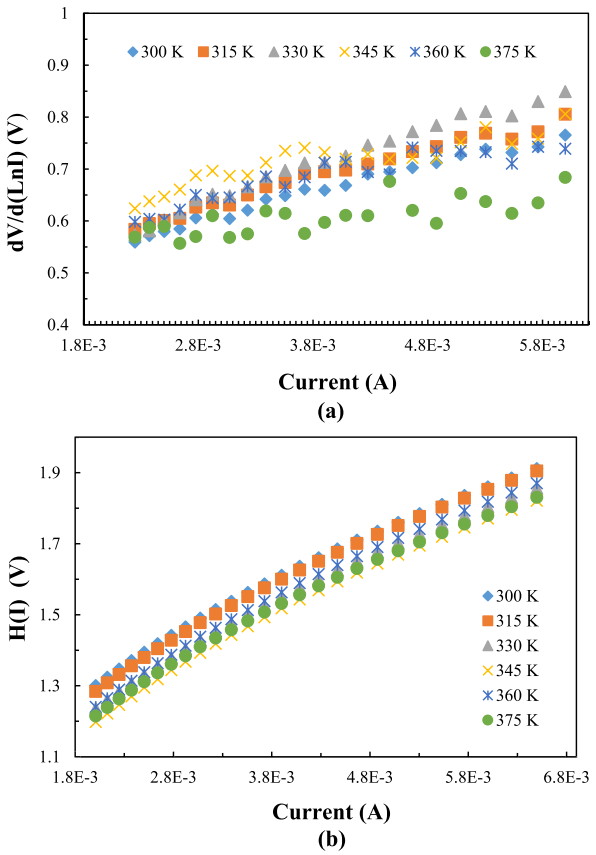

Fig. 4. (a) dV/d(LnI) versus current plot for Au/P3HT:PCBM/n-6H–SiC/Ag MPS SBD at different temperatures. (b) H(I) versus current plot for Au/P3HT:PCBM/n-6H–SiC/Ag MPS SBD at different temperatures.

PCBM/n-6H–SiC/Ag MPS SBD may be explained by increase of charge carrier concentration in the interface [33].

Another method used to find barrier height is the Richardson curves [34,35]. The expression of the equation that gives curves is

$$ln\left(\frac{I_0}{T^2}\right) = ln(AA^*) - \frac{q\Phi_{b0}}{kT}. \tag{10}$$

Richardson's plot $\ln(I_0/T^2)$ versus 1000/T determined from results in Eq. (10) is expected to be a linear straight line. The barrier height (Φ_{b0}) corresponding to activation energy at 0 K is found from the slope of this plot while Richardson constant (A*) is determined

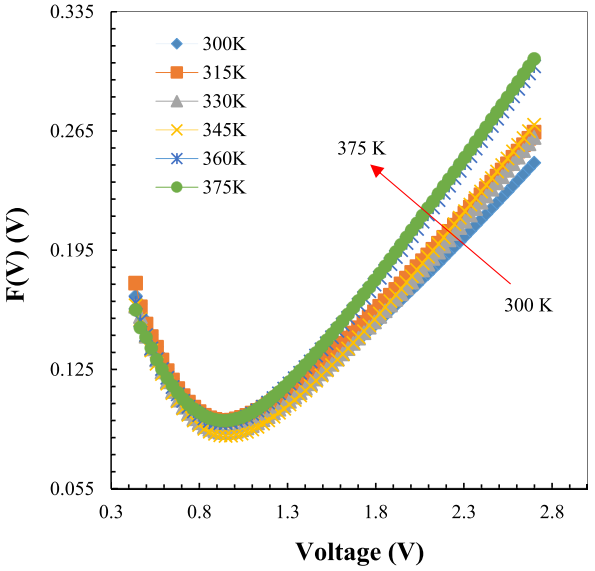

Fig. 5. Norde function versus voltage plot for Au/P3HT:PCBM/n-6H–SiC/Ag MPS SBD at different temperatures.

from the cutting point of the y-axis. Φ_{b0} and A* of Au/P3HT:PCBM/n-6H–SiC/Ag structure at zero-bias presented in Fig. 6 are determined as 1.65 eV and 3.03×10^{-12} $Acm^{-2}K^{-2}$, respectively. In Fig. 6, change of barrier height linearly with ideality factor shows that barrier height is inhomogeneous [36]. Richardson constant values appear to be very different from 146 $Acm^{-2}K^{-2}$ value known for 6H–SiC. Similar results have been found in other studies on 6H–SiC [15–17,37]. The Richardson constants obtained in these studies are found as 0.32, 21.21, 6.11×10^{-5} and 5.44×10^{-7} $Acm^{-2}K^{-2}$, respectively. The reason for deviations in Richardson's plot may be due to barrier height inhomogeneity or from potential fluctuations at the interface where low and high barrier regions are formed [38,39]. Another reason may be that Richardson constant (A*) derived from the experimental I–V analysis is different from spatial homogeneity of the barrier or actual effective mass from the calculated value [40]. In many studies, it is observed that barrier height decreases with decreasing temperature, on the contrary, the ideality factor increases [35,41]. One of the reasons for this situation is that it consists of different inhomogeneous barrier heights in the interface layer [17,42,43].

According to Tung, the ideality factor (n) has a linear relationship with zero-bias barrier height (Φ_{b0}) [35]. The plot drawn from the experimental results and the relation between Φ_{b0} and n is shown in Fig. 7. Inhomogeneous barrier heights are derived from the plot intercepting barrier height axis for n = 1. Accordingly, barrier height between 300 and 375 K temperatures for Au/P3HT:PCBM/n-6H–SiC/Ag MPS SBD was found 1.26 eV. When the plot in Fig. 7 is examined, the linear change of barrier height with ideality factor indicates that barrier height is inhomogeneous or irregular charge distribution in diode region.

Gaussian distribution (GD) model was defined by Song et al. in order to explain deviations of the experimental parameters calculated in TE model [44]. According to this model, it is shown that barrier height is inhomogeneous as the reason for deviation in I–V parameters. A model has been proposed by Werner and Güttler for the analysis of inhomogeneous barrier [45,46]. The inhomogeneity defined by Gauss distribution is described by

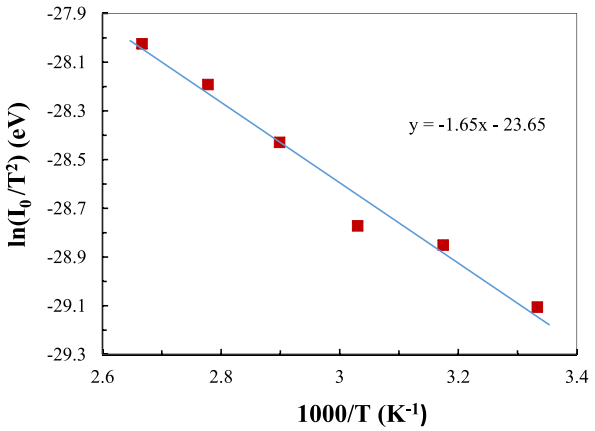

Fig. 6. Richardson's plot $\ln(I_0/T^2)$ versus 1000/T for Au/P3HT:PCBM/n-6H–SiC/Ag MPS SBD.

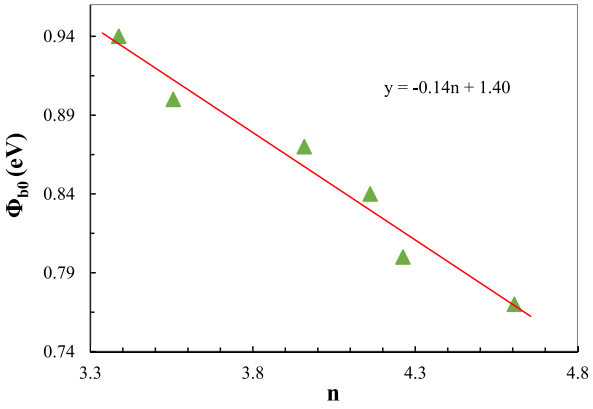

Fig. 7. Φ_{b0} versus n plot for Au/P3HT:PCBM/n-6H–SiC/Ag structure.

$$\Phi_{ap} = \overline{\Phi}_{bo}(T=0) - \frac{q\sigma_0{}^2}{2kT}, \tag{11}$$

where experimental barrier height is Φ_{ap}, standard deviation is σ_0 and mean barrier height is $\overline{\Phi}_{bo}$. In calculation of barrier height, temperature dependence of standard deviation (σ_0) may be neglected since it generally has a small value [45]. In the same model, the relation between ideality factor and temperature is

$$\left(\frac{1}{n_{ap}} - 1\right) = -\rho_2 + \frac{q\rho_3}{2kT}, \tag{12}$$

where the experimentally obtained ideality factor is n_{ap}, ρ_2 and ρ_3 are voltage constants. These factors that depend on the temperature have a linear relation with modified mean barrier height and ideal deviation parameters such as $\overline{\Phi}_b = \overline{\Phi}_{b0} + \rho_2 V$ and $\sigma_S = \sigma_0 + \rho_3 V$. In particular, small standard deviation means that barrier height is more homogeneous.

According to GD, inhomogeneity analysis of barrier height of the sample is determined by Eq. (11) and Eq. (12). The experimental Φ_{ap} and n_{ap}^{-1}-1 versus q/2 kT plot is shown in Fig. 8. According to the data derived from Eq. (11), the slope of Φ_{ap} versus q/2 kT plot gives standard deviation while the intersection of this plot on y-axis gives mean barrier height. The mean barrier height ($\overline{\Phi}_{bo}$) and standard deviation (σ_0) values at zero-bias at 300–375 K temperature range are obtained as 1.61 eV and −0.04, respectively. Again, according to the data obtained from Eq. (12), the slope of n_{ap}^{-1}-1 versus q/2 kT plot gives ρ_3 voltage constant while the intersection of this plot on y-axis gives ρ_2 voltage constant. The constants of ρ_2 and ρ_3 fit on the plot are 0.39 and −0.02, respectively. The reason why barrier height shows Gaussian distribution may be explained by inhomogeneity of charge distributions that consists of barrier [47]. This may be because of interface structure differences, interface quality, electrical charges in the interface and sensitivity of devices measuring at the nanoscale.

When Richardson equation is modified using saturation current in Eq. (2) and barrier height in Eq. (11) is defined as

$$ln\left(\frac{I_0}{T^2}\right) - \left(\frac{q^2\sigma^2}{2k^2T^2}\right) = ln(AA^{**}) - \frac{q\overline{\Phi}_{b0}}{kT}. \tag{13}$$

The modified effective Richardson's plot of Au/P3HT:PCBM/n-6H–SiC/Ag structure is presented in Fig. 9. Again, this plot gives a linear straight line. According to data calculated in Eq. (13), from the slope of Fig. 9 is found the mean barrier height ($\overline{\Phi}_{bo}$) and from the intersection of y-axis is determined the modified effective Richardson constant (A**). $\overline{\Phi}_{bo}$ and A** of the sample are figured out 1.53

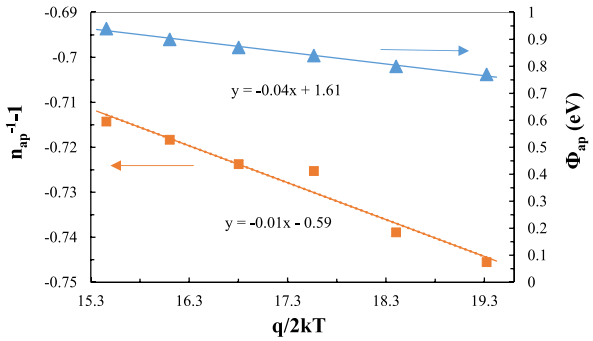

Fig. 8. Φ_{ap} and n_{ap}^{-1}-1 versus q/2kT plot for Au/P3HT:PCBM/n-6H–SiC/Ag structure.

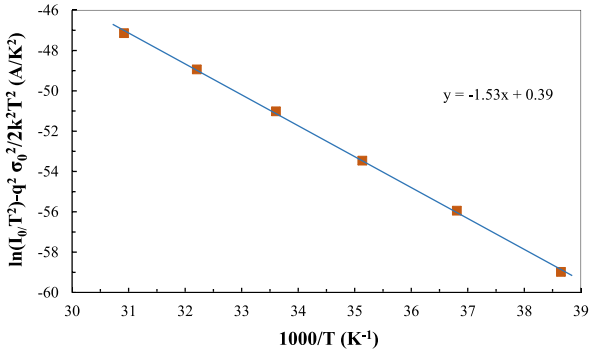

Fig. 9. The modified effective Richardson's plot of $\ln(I_0/T^2)$-$q^2\sigma_0^2/2k^2T^2$ versus 1000/T for Au/P3HT:PCBM/n-6H–SiC/Ag structure.

eV and 84.39 $Acm^{-2}K^{-2}$ at 300–375 K temperature range, respectively. The calculated values are in good agreement with theoretically known values for 6H–SiC [26].

Apart from current conduction models, the electrical characteristics of the fabricated sample are affected by interface material and interface state density. Particularly, interface state density (N_{ss}) plays an important role in calculating Φ_{b0} and n. When the interface layer thickness between metal and semiconductor increases, the probability of current conduction is reduced. Thus, the effective barrier height (Φ_e) shows an alteration depending on applied voltage [48]. The effective barrier height expression (Φ_e) is

$$\Phi_e = \Phi_{b0} + \left(1 - \frac{1}{n(V)}\right), \tag{14}$$

where the variation of effective barrier height depending on the voltage is $\beta = 1-1/n(V)$. Besides, the value of n(V) expressing ideality factor that changes with voltage is defined by Card and Rhoderick [49]. Accordingly, n(V) and interface state density (N_{ss}) are

$$n(V) = 1 + \frac{\delta}{\varepsilon_i}\left[\frac{\varepsilon_s}{W_d} + N_{ss}(V)\right], \tag{15}$$

$$N_{ss}(V) = \frac{1}{q}\left[\frac{\varepsilon_i}{\delta}(n(V) - 1) - \frac{\varepsilon_s}{W_d}\right], \tag{16}$$

in which ε_i and ε_s are dielectric constant of interface and semiconductor, respectively. The width of depletion region is W_d and thickness of interface layer is δ. The difference between conductivity band boundary of semiconductor (E_c) and interface state density energy (E_{ss}) is given by

$$E_c - E_{ss} = q(\Phi_e - V), \tag{17}$$

where charge of electron is q, effective barrier height is Φ_e, applied voltage is V. Thickness of interface layer for the sample is $\delta = 140$ nm, and dielectric constants of interface and semiconductor are $\varepsilon_i = 3.7\ \varepsilon_0$ and $\varepsilon_s = 9.6\ \varepsilon_0$, respectively. Here, dielectric constant of cavity is taken as $\varepsilon_0 = 8.85 \times 10^{-14}$ F/cm. As a function of voltage, n(V) and interface state density (N_{ss}) are calculated from Eq. (15) and Eq. (16). Also, the values of E_c-E_{ss} is obtained from Eq. (17). The plot of the experimental interface state density versus E_c-E_{ss} is presented in Fig. 10. N_{ss} takes the greatest value of 1.13×10^{12} ($eV^{-1}cm^{-3}$) at 300 K. N_{ss} decreases and E_c-E_{ss} increases as the temperature increases. This indicates that the characteristics of a diode are improving and ideality factor as a function of temperature is decreasing. The reason for the decrease of the interface state density as the temperature increases can be expressed by the barrier inhomogeneity between metal and semiconductor, blending ratio of P3HT:PCBM polymer interface layer and temperature dependence of ideality factor. Again, N_{ss} values change with forward bias depending on the position in the semiconductor bandgap. According to Fig. 10, N_{ss} values decrease as a linear up to 0.55 eV with a bias towards the below of conduction band. But, E_c-E_{ss} values after 0.55 eV in the plot seem to increase N_{ss} similar to exponential. Besides, the variation of this parameter may depend on the existence of the polymer layer, which can prevent diffusion current between Au contact and n-SiC surface. N_{ss} values of sample produced using P3HT:PCBM blend as the interface layer are lower compared to other studies on Au/n-Si and Au/P3HT:PCBM/n-Si Schottky barrier diodes in the literature [23,24,50,51]. The reason for the lower N_{ss} value may be that the P3HT:PCBM blend between metal contacts and SiC reduces the transition current, or lower barrier heights located at the interface between metal and polymer. Hence, the fabricated Au/P3HT:PCBM/n-6H–SiC/Ag structure is very suitable for electronic and optoelectronic devices that require high quality.

4. Conclusion

In summary, essential electrical parameters of fabricated Au/P3HT:PCBM/n-6H–SiC/Ag Schottky barrier diode such as barrier height (Φ_{b0}), ideality factor (n), series resistance (R_s) and interface state density (N_{ss}) obtained from I–V measurements have been investigated at 300–375 K temperature range. The dependence of ideality factor and barrier height on temperature reveals the

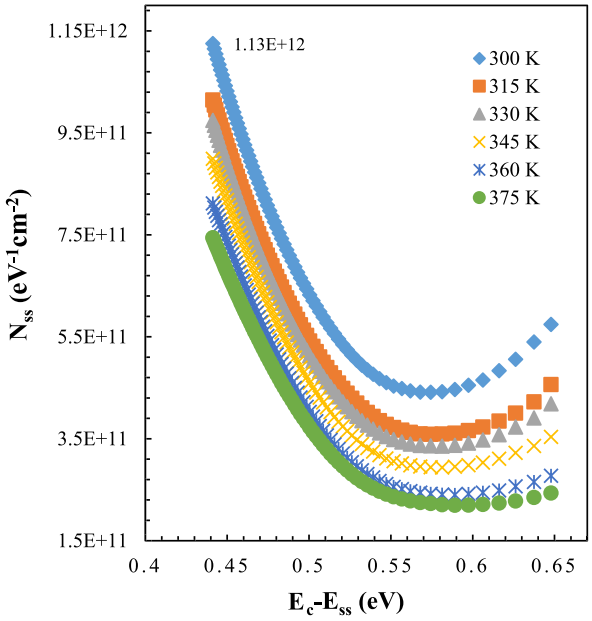

Fig. 10. Interface state density (N_{ss}) versus E_c-E_{ss} plot for Au/P3HT:PCBM/n-6H–SiC/Ag structure.

presence of inhomogeneous barrier formation. R_s values of the sample are found in two different ways using Cheung-Cheung and Norde methods. It is observed that series resistances obtained by different methods are in harmony for contacts. Considering the found series resistance values, series resistance increases with decreasing temperature. As a reason, it can be said that ideality factor increases with a decrease in temperature, free carrier concentration decreases and the polymer layer has an effect. According to the experimentally obtained data, the mean barrier heights ($\overline{\Phi}_{bo}$) have different standard deviation (σ_0) values at different temperatures. From calculated standard deviation values, $\overline{\Phi}_{bo}$ and the modified effective Richardson constant (A**) are recalculated and these parameters have a very good agreement with its known theorical value. Finally, it is concluded that N_{ss} decreases with increasing temperature. This is explained by the fact that the barrier between metal and semiconductor is inhomogeneous and temperature dependence of ideality factor.

Declaration of competing interest

The authors declare that they have no known competing financial interests or personal relationships that could have appeared to influence the work reported in this paper.

Acknowledgments

We would like to thank Associate Professor Doctor Özge Tüzün Özmen, Doctor Hüseyin Muzaffer Şağban and Professor Doctor Selim Acar for their help to this study.

Appendix A. Supplementary data

Supplementary data to this article can be found online at https://doi.org/10.1016/j.spmi.2020.106658.

References

[1] P. Mahala, S.K. Behura, A.S. Kushwaha, A. Ray, O. Jani, C. Dhanavantri, Semicond. Sci. Technol. 28 (2013), 055012.
[2] S.O. Tan, J. Polytech. 21 (2018) 977–989.
[3] İ. Taşçıoğlu, Ö.T. Özmen, H.M. Şağban, E. Yağlıoğlu, Ş. Altındal, J. Electron. Mater. 46 (2017) 2379–2386.
[4] S.K. Gupta, B. Shankar, W.R. Taube, J. Singh, J. Akhtar, Physica B 434 (2014) 44–50.
[5] T. Marinova, A.K. Georgieva, V. Krastev, R. Kakanakov, M. Neshev, L. Kassamakova, O. Noblanc, C. Arnodo, S. Cassette, C. Brylinski, Mater. Sci. Eng. B 46 (1997) 223–226.
[6] M. Benamara, M. Anani, B. Akkal, Z. Benamara, J. Alloys Compd. 603 (2014) 197–201.
[7] F. Roccaforte, F. La Via, V. Raineri, R. Pierobon, E. Zanoni, J. Appl. Phys. 93 (2003) 9137–9144.
[8] A.S. Mukasyan, Silicon Carbide: Synthesis and Properties, Combustion Synthesis of Silicon Carbide, 2011, pp. 336–338.

[9] H. Abderrazak, E.S. Hmida, Silicon Carbide: Synthesis and Properties, Properties and Applications of Silicon Carbide, 2011, pp. 362–368.
[10] M. Badila, G. Brezeanu, J. Millan, P. Godignon, M.L. Locatelli, J.P. Chante, A. Lebedev, P. Lungu, G. Dinca, V. Banu, G. Banoiu, Diam. Relat. Mater. 9 (2000) 994–997.
[11] S.R. Kodigala, S. Chattopadhyay, C. Overton, I. Ardoin, B.J. Gordon, D. Johnstone, D. Roy, D. Barone, Appl. Surf. Sci. 330 (2015) 465–475.
[12] C.L. Zhu, Rusli, P. Zhao, Solid State Electron. 51 (2007) 343–346.
[13] M.T. Soo, K.Y. Cheong, A.F. Noor, Sensor. Actuator. B 151 (2018) 39–55.
[14] S. Asubay, M.F. Genisel, Y.S. Ocak, Mater. Sci. Semicond. Process. 28 (2014) 94–97.
[15] K. Ejderha, A. Karabulut, N. Turkan, A. Turut, Siliconindia 9 (2017) 395–401.
[16] L. Boussouar, Z. Ouennoughi, N. Rouag, A. Sellai, R. Weiss, H. Ryssel, Microelectron. Eng. 88 (2011) 969–975.
[17] T. Güzel, A.K. Bilgili, M. Özer, Superlattice. Microst. 124 (2018) 30–40.
[18] A.F. Özdemir, D.A. Aldemir, A. Kökçe, S. Altındal, Synth. Met. 159 (2009) 1427–1432.
[19] F.C. Krebs, Polymeric Solar Cells; Materials, Design, Manufacture, DEStech Publications, Inc., Lancaster, PA, USA, 2010.
[20] M. Punke, S. Mozer, M. Stroisch, M. Gerken, G. Bastian, U. Lemmer, D.G. Rabus, P. Henzi, Proc. SPIE 6185 (2006) 618505.
[21] R. De Bettignies, J. Leroy, M. Firon, C. Sentein, Synth. Met. 156 (2006) 510–513.
[22] G. Paternó, F. Cacialli, V. García-Sakai, Chem. Phys. 427 (2013) 142–146.
[23] Ö.T. Özmen, Microelectron. Reliab. 54 (2014) 2766–2774.
[24] Ö.T. Özmen, E. Yağlıoğlu, Mater. Sci. Semicond. Process. 26 (2014) 448–454.
[25] S.M. Sze, Physics of Semiconductor Devices, New Jersey, third ed., 2007.
[26] F.E. Cimilli, H. Efeoğlu, M. Sağlam, A. Türüt, J. Mater. Sci. Mater. Electron. 20 (2009) 105–112.
[27] A.A. Kumar, L.D. Rao, V.R. Reddy, C.J. Choi, Curr. Appl. Phys. 13 (2013) 975–980.
[28] J. Chen, Q. Wang, J. Lv, H. Tang, X. Li, J. Alloys Compd. 649 (2015) 1220–1225.
[29] H.H. Güttler, J.H. Werner, Appl. Phys. Lett. 56 (1990) 1113–1115.
[30] H. Norde, J. Appl. Phys. 50 (1979) 5052–5053.
[31] M. Yasin, T. Tauqeer, K.S. Karimov, S.E. San, A. Kösemen, Y. Yerli, A.V. Tunc, Microelectron. Eng. 130 (2014) 13–17.
[32] S.K. Cheung, N.W. Cheung, Appl. Phys. Lett. 49 (1986) 85–87.
[33] S. Chand, J. Kumar, Appl. Phys. A 63 (1996) 171.
[34] A.S. Bhuiyan, A. Martinez, D. Esteve, Thin Solid Films 161 (1988) 93–100.
[35] R.T. Tung, Phys. Rev. B Condens. Matter 45 (1992) 13509–13523.
[36] J.R. Waldrop, R.W. Grant, Y.C. Wang, R.F. Davis, J. Appl. Phys. 72 (1992) 4757–4760.
[37] W. Yue-Hu, Z. Yi-Men, Z. Yu-Ming, S. Qing-Wen, J. Ren-Xu, Chin. Phys. B 20 (2011), 087305.
[38] S. Chand, J. Kumar, Appl. Phys. A 65 (1997) 497–503.
[39] W.P. Kang, J.L. Davidson, Y. Gurbuz, D.V. Kerns, J. Appl. Phys. 78 (1995) 1101–1107.
[40] J. Osvald, Z.S. Horvath, Appl. Surf. Sci. 234 (2004) 349–354.
[41] J.P. Sullivan, R.T. Tung, M.R. Pinto, W.R. Graham, J. Appl. Phys. 70 (1991) 7403–7424.
[42] A.K. Bilgili, T. Güzel, M. Özer, J. Appl. Phys. 125 (2019) 35704, 0.
[43] R.F. Schmitsdorf, T.U. Kampen, W. Monch, Surf. Sci. 324 (1995) 249–256.
[44] Y.P. Song, R.L. van Meirhaeghe, W.H. Laflére, F. Cardon, Solid State Electron. 29 (1986) 633–638.
[45] J.H. Werner, H.H. Güttler, J. Appl. Phys. 69 (1991) 1522.
[46] J.H. Werner, H.H. Güttler, Phys. Scripta T39 (1991) 258.
[47] P. Cova, A. Singh, Solid State Electron. 33 (1990) 11–19.
[48] H. Benmaza, B. Akkal, H. Abid, J.M. Bluet, M. Anani, Z. Bensaad, Microelectron. J. 39 (2008) 80–84.
[49] H.C. Card, E.H. Rhoderick, J. Appl. Phys. D 4 (1971) 1589–1601.
[50] S. Alialy, H. Tecimer, H. Uslu, S. Altindal, 1000167, J. Nanomed. Nanotechnol. 4 (2013) 1–7.
[51] M. Gökçen, T. Tunç, Ş. Altındal, İ. Uslu, Curr. Appl. Phys. 12 (2012) 525–530.